physica status solidi a
www.pss-a.com

Check for updates

Toward Magneto-Plasmonic Functionality in a Self-Assembled Device Based on Colloidal Synthesis

Siavash Qodratipour, Henry Halim, Martin Rothe, Günter Kewes, Yan Lu, and Oliver Benson*

The confinement of surface plasmon polaritons (SPPs) offers strong field strengths also for longitudinal field components. Phenomena like spin-momentum locking can thus be exploited for novel functionality in nanodevices. External control of transport or directional coupling of propagating SPPs would be highly interesting for applications. Herein, the coupling of noble metal and magnetic nanoparticles to a silver nanowire acting as SPP waveguide using a hybrid self-assembly approach is demonstrated. A designated setup is reported to isolate and investigate magnetically controlled transport in such devices. Various configurations are measured to quantify the required sensitivity for the typically tiny magnet response at moderate strengths of the magnetic field. Although magnetic control cannot be achieved, the required improvements can be estimated based on a heuristic numerical model. It is suggested using an approach to enhance magnetic response using a combination of metal and magnetic nanoparticles. Such devices can be assembled in principle with self-assembly approach in a multistep process.

1. Introduction

The strong confinement of the electromagnetic field in surface plasmon polaritons (SPPs) offers new ways to implement novel or enhanced functionality in nanodevices. Especially, near-field phenomena can be exploited. Spin-momentum locking (SML) is a phenomenon that links the propagation direction of optical fields with its angular momentum. Several applications of SML have been proposed or realized.[1–16] Since SML relies on longitudinal field components in the near-field, strong confinement of a propagating mode is crucial. Recently, we introduced a concept for detecting the chiral response of molecules using a silver nanowire as a plasmonic waveguide and a plasmonic nanoantenna to create a sensing hot spot.[17] In this contribution, we envision another SML-based application, i.e., routing of electromagnetic fields in a self-assembled device controlled via magnetic fields.[18–26]

The article is structured as follows: In Section 2, we start by introducing the conceptual idea of our envisioned magneto-plasmonic router. Then, in Section 3, we describe our synthesis of the various nanoparticles and nanowires for self-assembly of the device. Section 4 shows that self-assembly of different device architectures is indeed possible. We then present experimental studies in Sections 5 and 6 on implementing magneto-plasmonic functionality using gold nanospheres and potential enhancement of the magneto-plasmonic response with iron oxide nanoclusters, respectively. Sensitivity estimations of future devices conclude our article.

2. Working Principle of a Magneto-Plasmonic Waveguide Router

2.1. General Routing Principle

Figure 1 sketches the concept of magnetically controlled plasmon routing. A silver nanowire acts as a waveguide for surface plasmon polaritons (SPPs). The accessible near-field is controlled by the cross-section and a dielectric coating of the wire. Due to the strong field confinement, guided modes are not purely transversal, but contain longitudinal components in the near-field. A nanoparticle in the near-field scatters impinging laser light into propagating SPPs. Spin-momentum locking provides a correlation between circularly polarized components of the laser light and the propagation direction of the SPPs.[27] If the laser is linearly polarized, right and left propagating SPP modes are equally excited (Figure 1a). However, if the scatter has a chiral response, e.g., if it shows circular dichroism an imbalance between right or

S. Qodratipour, M. Rothe, G. Kewes, O. Benson
Institut für Physik & IRIS Adlershof
Humboldt-Universität zu Berlin
Newtonstraße 15, 12489 Berlin, Germany
E-mail: qodratis@physik.hu-berlin.de

H. Halim, Y. Lu
Department for Electrochemical Energy Storage (CE-AEES)
Helmholtz Zentrum Berlin für Materialien und Energie
Hahn-Meitner-Platz 1, 14109 Berlin, Germany

Y. Lu
Institut für Chemie
University of Potsdam
14476 Potsdam, Germany

The ORCID identification number(s) for the author(s) of this article can be found under https://doi.org/10.1002/pssa.202300380.

© 2023 The Authors. physica status solidi (a) applications and materials science published by Wiley-VCH GmbH. This is an open access article under the terms of the Creative Commons Attribution License, which permits use, distribution and reproduction in any medium, provided the original work is properly cited.

DOI: 10.1002/pssa.202300380

© 2023 The Authors. physica status solidi (a) applications and materials science published by Wiley-VCH GmbH

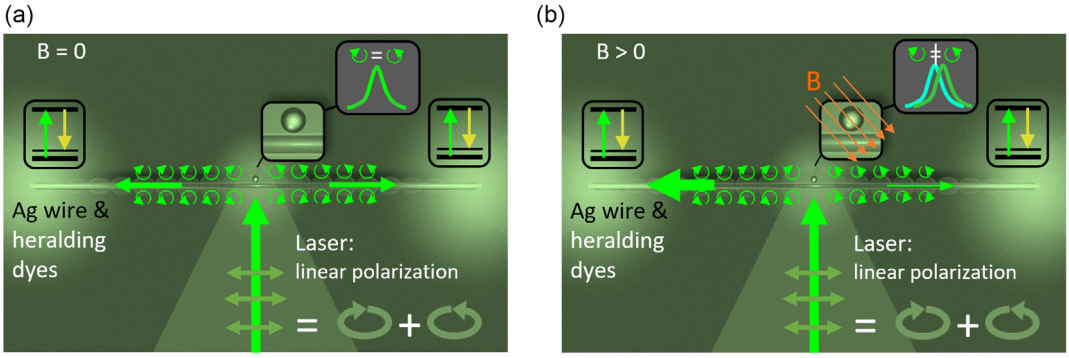

Figure 1. Schematics of a magnetically controlled plasmon router. a) A gold nanosphere representing a plasmonic antenna concentrates incident linearly polarized light in a hot spot next to a silver nanowire acting as a plasmonic waveguide. Surface plasmon polaritons (SPPs) are launched both to the left and to the right side of the waveguide. Far-field detection of SPPs is facilitated by Stokes-shifted fluorescence from dye molecules contained in a silica shell surrounding the nanowire. b) Spin-momentum locking correlates circularly polarized components of the incident light field and the SPP propagation direction. If an external magnetic field induces circular dichroism in the gold nanosphere, then the elliptical polarization of the near-field leads to a preferential SPP propagation direction.

left polarized field components leads to an imbalanced generation of SPP modes.

As an example in Figure 1b, more SPPs are propagating to the left than to the right. A gold nanosphere represents a resonant scattering particle. At the same time, it shows magnetic circular dichroism (MCD), i.e., a chiral response under the presence of a magnetic field. MCD in a Drude metal particle in the presence of an external magnetic field can be understood following Gabbani et al.[28] When circularly polarized light excites the plasmonic oscillation, one can think of a circular motion of free electrons, which degenerates for the two helicities in the absence of a magnetic field. When a magnetic field is applied the Lorentz force accelerates or decelerates the clockwise or anticlockwise motion. Consequently, the degeneracy of the plasmonic modes is removed and the resonance conditions of a localized surface plasmon resonance peak for right and left circularly polarized light, respectively, are shifted. An inversion of the magnetic field is equivalent to reversing the handedness of the circularly polarized light.[28–31] MCD introduced by an external magnetic field is indicated in Figure 1b by the red magnetic field lines of field *B*.

Overall the role of the gold nanosphere is twofold. First, it can enhance incoming light significantly in hot spots by acting as a resonant plasmonic antenna. Second, it provides a chiral response that is controllable by a magnetic field. Overall, the combination of a silver nanowire and a gold nanosphere allows for control of SPP propagation direction, i.e., magnetic routing of SPPs.[32] The switching contrast of the directional coupling depends on the strength of the magneto-plasmonic response and on the wavelength of the excitation light. Tailored nanoparticles with a gold core and an iron oxide shell (or vice versa) can enhance the contrast since the magnetization of iron oxide leads to a strong enhancement of local magnetic fields.[33,34]

In our device architecture, we also address the technical problem of detecting SPPs with a good signal-to-noise ratio. At both ends, facets of the nanowire SPPs are scattered into photons and in principle can be detected in the far field. However, the exciting laser light typically overshines these scattered photons. Our nanowire waveguides have a thin silica shell hosting fluorophores (3,4,9,10-perylenetetracaboxylic dianhydride dye molecules) (**Figure 2**a,b). They can absorb plasmons and emit a Stokes-shifted fluorescence. Spectral filtering can then suppress the excitation laser light significantly.

To induce a chiral response of the gold nanosphere we use a strong permanent magnet positioned on top of our sample. A future more integrated device may contain a re-writable magnetic domain directly on the chip. We discuss the magneto-plasmonic effect of gold nanospheres in Section 5.1.

The contrast or visibility of this unbalanced directional coupling depends not only on the strength of the magneto-plasmonic effect but also on the wavelength of the excitation light. For our device, a variety of nanoparticles can be used, such as bare gold nanospheres or hybrid core-shell particles with an iron oxide (Fe_3O_4) (Figure 2c) around gold (or vice versa). The hybrid particles have the advantage that iron oxide is easily magnetized which might yield a stronger magnetic field in the very proximity of the gold nanosphere.

2.2. Strategy for Self-Assembly

Hybrid devices integrate vastly different materials to achieve a novel or superior functionality.[35] This imposes a big challenge on fabrication, since the different fabrication methods for individual constituents may be incompatible. One approach is manual assembly using micromanipulation.[36,37] The advantage lies in the precise control and versatility, however, it is not a scalable approach and is only suitable for proof-of-principle demonstrations. Another approach is self-assembly.[38] This approach has been very successful and in combination with colloidal synthesis[39] is also cost-efficient. Since our device requires the combination of nanostructures with plasmonic features and magnetic response we utilize self-assembly. Figure 2 illustrates our approach. We start with individual building blocks such as nanowires, nanospheres, and nanoparticles fabricated by colloidal synthesis. After drop-casting or spin-coating solutions containing such particles, self-assembly leads to the formation of functional devices on, e.g., glass substrates. Then, we select successfully formed devices and study their functionality. The process may consist of multiple steps if different nanoparticles are involved.

© 2023 The Authors. physica status solidi (a) applications and materials science published by Wiley-VCH GmbH

18626319, 0, Downloaded from https://pericles.pericles-prod.literatumonline.com/doi/10.1002/pssa.202300380 by Helmholtz-Zentrum Berlin Für, Wiley Online Library on [12/12/2023]. See the Terms and Conditions (https://onlinelibrary.wiley.com/terms-and-conditions) on Wiley Online Library for rules of use; OA articles are governed by the applicable Creative Commons License

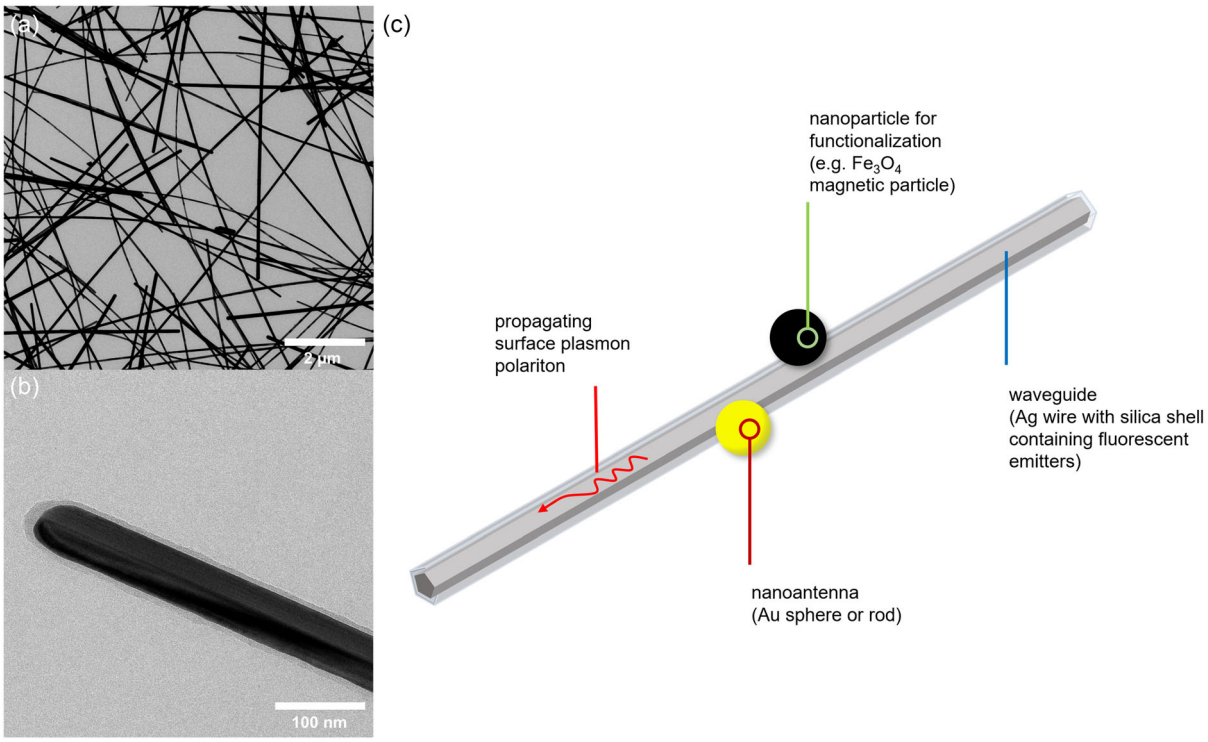

Figure 2. Schematic of self-assembly approach of a magneto-plasmonic device. a) TEM image of silver nanowires acting as plasmonic waveguides (scale bar is 2 µm). b) Closeup of silica-coated nanowires with a smooth, thin silica shell (scale bar is 100 nm). c) General idea of combining waveguides and different colloidal particles (metal spheres as plasmonic antennas and magnetic nanoparticles or nanoclusters) to introduce magneto-plasmonic functionality.

3. Optimized Synthesis of Device Constituents

3.1. Plasmonic Waveguides

3.1.1. Silver Nanowires

Silver nanowires with a diameter of 70 nm and average length of 5 µm were synthesized by a polyol method.[40] Here, poly(N-vinylpyrrolidone) is dissolved in ethylene glycol and is heated to 160 °C. Then, a small amount of sodium chloride solution was added and finally silver nitrate solution in ethylene glycol. Although the reaction appears simple at first glance, numerous empirical and simulation studies have been done to try to explain the role of each reagent and the mechanism behind the nanowire formation with varying success.[41–45] Recently, Jharimune et al.[46] discovered that the mechanism is rather complex and also involves the chemical identity and concentration of the poly(N-vinylpyrrolidone) end groups. Silver nanowire synthesis has also been optimized by a two-step injection process[40] allowing for the production of wires in large quantities.

3.1.2. Silica Coating Containing Fluorescent Molecules

As discussed in the previous section, the detection of SPPs is facilitated by Stokes-shifted fluorescence from dye molecules in a thin silica shell around the silver nanowires. A thin shell (≈7 nm) is necessary to preserve the plasmonic properties of the nanowires. The silica shell can be synthesized by the Stöber method, however, a precise control of the process is necessary to achieve a smooth shell without roughening the silver surface by etching. One way to do this is to use our modified Stöber method, which uses sodium hydroxide instead of ammonium hydroxide.[47] This minimizes the damage from etching and allows for the formation of high-quality silica shell on the nanowires. To embed fluorescent molecules in the silica shell, a small amount of 3,4,9,10-perylenetetracaboxylic dianhydride dye molecules was simply introduced in the ethanol solvent during the coating process.[17,48] Figure 2a,b shows TEM images of the synthesized core-shell silver nanowires revealing the smooth, thin silica shell.

3.2. Nanoantenna and Magnetic Functionality

3.2.1. Plasmonic Nanoparticle

In our device concept, a gold nanosphere acts as a plasmonic antenna to concentrate the excitation light in a local hot spot next to the silver nanowire. There, SPPs are generated and propagated along the silver nanowire acting as a plasmonic waveguide. We synthesized gold nanospheres by reduction of gold chloride.[49] First, small gold nuclei are synthesized by boiling an aqueous solution of sodium citrate, and then a solution of gold chloride is introduced. These nuclei act as seeds, which can grow to larger

© 2023 The Authors. physica status solidi (a) applications and materials science published by Wiley-VCH GmbH

18626319, 0, Downloaded from https://particles.particles-prod.literatumonline.com/doi/10.1002/pssa.202300380 by Helmholtz-Zentrum Berlin Für, Wiley Online Library on [12/12/2023]. See the Terms and Conditions (https://onlinelibrary.wiley.com/terms-and-conditions) on Wiley Online Library for rules of use; OA articles are governed by the applicable Creative Commons License

gold nanospheres at lower temperatures (90 °C). Stepwise growth of the gold nanospheres at lower temperatures prevents the formation of new nuclei, allowing relatively narrow size distribution and near-ideal spherical shape. The nanospheres can then be stochastically self-assembled with the nanowires through mixing, drop-casting, or spin-coating and eventually a drying process on a substrate. In this study, commercially available gold nanospheres from nanoComposix are used in the experiments.

3.2.2. Magnetic Nanoparticles

As pointed out in Section 2.1, the gold nanospheres provide magneto-plasmonic functionality through magnetic circular dichroism (MCD). MCD has been measured for various colloidal plasmonic particles,[28–31] however, the effect is very small and difficult to detect on the level of a single particle. Core-shell hybrid particles or two-particle clusters combining the properties of magnetic and plasmonic particles enhance magneto-plasmonic properties[50] for wavelengths near the plasmon resonance.[51] Due to the huge demand of magnetic nanoparticles for bioapplications, numerous synthetic methods are available.[52] Particle sizes can be well controlled and range between a few to a few tens of nanometers. Surface modification, e.g., by polymer coating can be applied to achieve dispersion of the nanoparticles in water. In this study, we performed several experiments with commercially available iron oxide (Fe_2O_4) nanoparticles or clusters from PlasmaChem. Gold-coated iron oxide nanoparticles[34] have shown plasmon-enhanced magneto-optical effects such as enhanced Faraday rotation. As indicated schematically in Figure 2c and discussed in Section 2.2, two-particle hybrid clusters of gold particles and iron oxide particles can be formed next to a nanowire plasmonic waveguide directly by self-assembly.

4. Self-Assembly and Device Characterization

4.1. Optical and Scanning SEM Investigation

We used a multipurpose wide-field microscopy setup to study individual nanoparticles and selected self-assembled devices. The setup is an inverted optical microscope, as shown in **Figure 3**a. For excitation, we use a white-light source (Xe lamp) and a cw laser (532 nm) with adjustable polarization via a half-wave plate, a quarter-wave plate, and a linear polarizer. Filters can be inserted before the detected light reaches a spectrometer, a color camera, or a cooled CCD camera. A rotatable permanent magnet is positioned on top of the sample to provide a static magnetic field. A magnetic field of up to 0.5 Tesla can be reached at a distance of 3 mm above the sample.

As a first example, Figure 3b,c shows dark-field scattering microscopy images of (b) 100 and (c) 50 nm diameter of gold nanospheres dispersed on a glass cover slide. Samples were prepared via spin-coating diluted gold particle solutions on the glass substrate. In the setup, identified nanospheres can be selected (examples are indicated by red circles to guide the eyes) and investigated further.

The self-assembled devices were prepared on glass substrates in two separate steps. First, the silver nanowire solution was placed in an ultrasonic bath for a short period of 3–5 min to

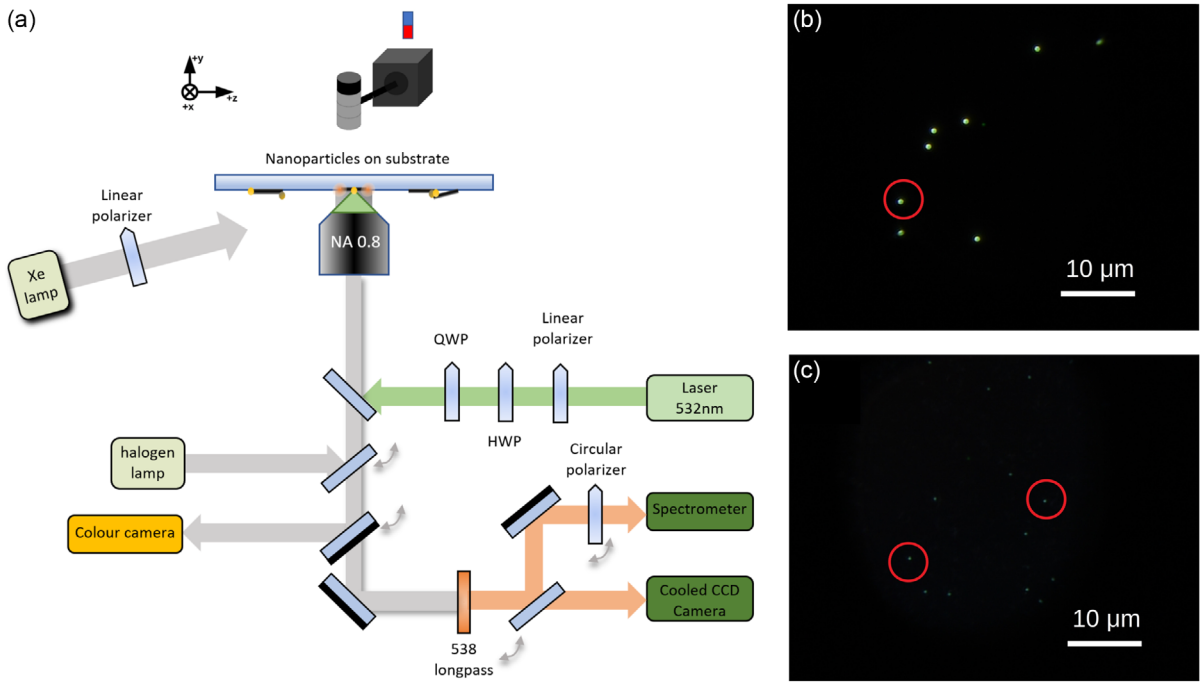

Figure 3. a) Multipurpose wide-field setup used for optical studies of various nanoparticles and selected self-assembled devices. A white-light source (Xe lamp) and a laser (532 nm) with adjustable polarization are used for illumination. Filters are inserted before detection with a spectrometer and at CCD camera. A rotatable permanent magnet above the sample provides a static magnetic field. b,c) Dark-field scattering microscopy images of 100 and 50 nm gold nanospheres, respectively. The red circles indicate selected particles for further studies.

© 2023 The Authors. physica status solidi (a) applications and materials science published by Wiley-VCH GmbH

18626319, 0, Downloaded from https://particles.pericles-prod.literatumonline.com/doi/10.1002/pssa.202300380 by Helmholtz-Zentrum Berlin Für, Wiley Online Library on [12/12/2023]. See the Terms and Conditions (https://onlinelibrary.wiley.com/terms-and-conditions) on Wiley Online Library for rules of use; OA articles are governed by the applicable Creative Commons License

de-cluster the nanowires. Later on, the nanowires were spin-coated on a cleaned substrate and dried under ambient conditions. Then, nanospheres or iron oxide nanoclusters were also placed in an ultrasonic bath. A proper density of the solution was then drop-casted on the glass substrate. The sample was spun after a few minutes of drying to achieve a more homogeneous distribution of particles. The coffee-ring effect[53] resulted in a suitable yield to find self-assembled devices. In this two-step deposition and self-assembly approach it is of crucial importance to identify individual nanoobjects on the substrate. To achieve this, we performed correlated SEM and dark-field imaging. The self-assembly was performed on silicon finder grid substrates. The suitable individual nanoobjects were identified via SEM imaging and the materials were further analyzed using energy discursive X-ray analysis (EDX). SEM images of the silicon finder grid substrate provide coordinates for the nanoobjects. The chosen nanoobjects then were located in the optical microscopy setup using dark-field imaging in correlation with the SEM images and their coordinates on the sample's grid.

Figure 4 shows correlated optical and SEM images of different self-assembled devices. Each device consists of a silver nanowire and a nanoparticle attached to it as a functional element.

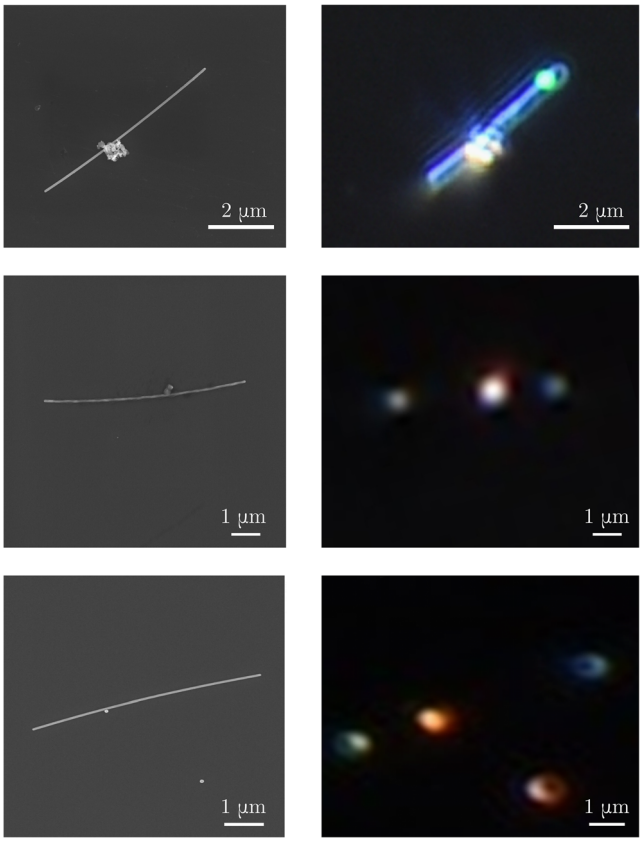

Figure 4. Correlated optical and SEM investigation of self-assembled devices. The left column shows SEM and the right column optical true-color dark-field microscopy images, respectively. A nanowire with a silica shell is functionalized with an iron oxide nanocluster (top row), a silver nanosphere (middle row), and a gold nanosphere (bottom row). The green spot (red arrow) in the first row shows the excitation laser.

The nanoparticles are gold nanospheres, silver nanospheres (to demonstrate the versatility of the self-assembly), and iron oxide nanoclusters. We would like to point out that the controllable thickness of the silica shell around the nanowire also provides a well-defined distance between the nanoparticles and the surface of the silver wire.

4.2. Spin-Momentum Locking in Self-Assembled Nanowire-Nanoparticle Systems

All combinations of nanoparticles and nanowires show the spin-momentum locking phenomenon. This is a very promising result as it proves that spin-locking is robust and that our assembly provides working devices with a high yield. As an example, we show a measurement with a silver nanosphere and a silver nanowire in **Figure 5**. We focussed the excitation laser (532 nm) on the nanoparticle and detected the SPPs traveling to both ends of the nanowire via the Stokes-shifted fluorescence of the molecules in the silica shell surrounding the wire. Details of such measurements with a gold nanosphere are described in Rothe et al.[17] When the polarization of the excitation laser is changed, a correlation between the polarization and the directionality of SPP propagating can be observed. However, we found changes in the contrast even for identical polarization. Further, an overall drift of the contrast with the time it took to perform the measurements can be observed. This is predominantly caused by the continuous bleaching of the fluorescent molecules in the nanowire's shell. This leads to continuous decrease in the detected signal. Since bleaching depends also on the history of previous laser illumination and since the nanoparticle is not positioned exactly in the middle of the wire, the contrast between the left and the right propagating signal can slightly change with time. Here, also an effect of the drift of the focus may set in. However, there is still an apparent modulation according to the change in the polarization of the excitation. Rather than fitting the data with a sinusoidal modulation with varying amplitude, we added a sinusoidal to indicate the degree of circular polarization of the excitation laser. Finally, we would like to point out that spin-locking depends on

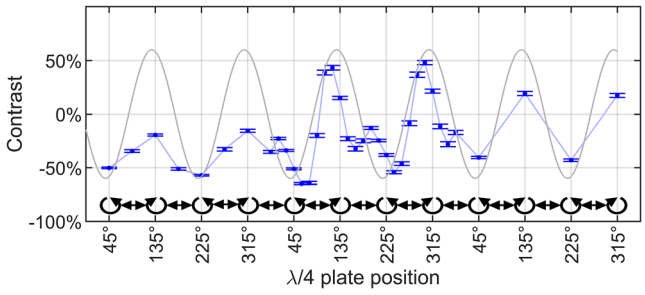

Figure 5. Measured contrast (blue dots) between SPPs detected at both end facets of a silver nanowire when light is focussed on a silver nanosphere attached to a silver nanowire. The configuration corresponds to the middle row of Figure 4. The polarization of the excitation laser is changed by rotating a $\lambda/4$-plate.[17] The solid gray line is sinusoidal indicating the degree of circular polarization when the $\lambda/4$-plate is rotated continuously. Changes in the amplitude of the modulated contrast are mainly due to the bleaching of the fluorescent molecules in the nanowire's shell (details discussed in text).

© 2023 The Authors. physica status solidi (a) applications and materials science published by Wiley-VCH GmbH

18626319, 0, Downloaded from https://pericles.pericles-prod.literatumonline.com/doi/10.1002/pssa.202300380 by Helmholtz-Zentrum Berlin Für, Wiley Online Library on [12/12/2023]. See the Terms and Conditions (https://onlinelibrary.wiley.com/terms-and-conditions) on Wiley Online Library for rules of use; OA articles are governed by the applicable Creative Commons License

the mode overlap of the scattering particle's resonant modes and the mode of propagating surface plasmon polaritons in the near-field. For larger particles (our iron oxide nanoclusters had a radius of up to 150 nm and an irregular shape), higher-order Mie modes (see Supporting Information) may deteriorate the contrast in spin-locking measurement.

5. Functionality via Magnetic Circular Dichroism

5.1. Magnetic Circular Dichroism in Spherical Metal Particles

As pointed out in Section 2.1, a gold nanosphere in a strong magnetic field already provides magnetic circular dichroism (MCD). For a spherical nanoparticle, three degenerate and mutually orthogonal plasmon modes exist. Two of them can be simultaneously excited by an incident linearly polarized light forming circularly polarized plasmon modes.[54] If an external magnetic field is applied parallel to the direction of light propagation, the degeneracy of the modes is lifted, and the resonance is splitted, as indicated in **Figure 6**. For a gold nanosphere, the relative shift of the absorption spectrum due to a magnetic field of 0.5 Tesla can be approximated to an amount of 10^{-3}% over the plasmon resonance frequency.[30] This shift can be used to estimate the shift of the dark-field scattering resonance for a 100 nm gold nanosphere. With the resonance at 556 nm, a spectral shift of 556×0.00001 nm is expected. **Figure 7** shows the calculated MCD spectrum, which is the difference of spectra for two antiparallel orientations of the magnetic field. The calculated MCD spectrum is detectable with a minimum signal-to-noise ratio (SNR) of 10^4 for the dark-field scattering spectra. Our experimental setup is described in Section 4.1 and the measurement parameters are modified to reach the desired SNR. This error range is indicated in Figure 7 as a gray-shaded area. The MCD signal from a single gold nanosphere is very weak but could be measurable in the lab in principle.

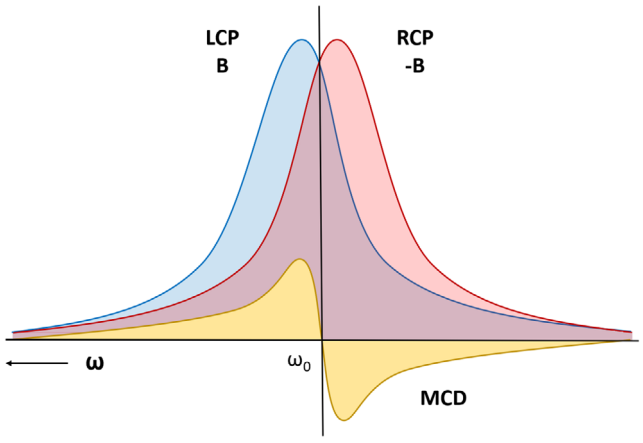

Figure 6. Schematic of the two circular plasmon modes (denoted LCP and RCP) excited with left circularly polarized light (blue spectrum) and right circularly polarized light (red spectrum) with a magnetic field parallel and antiparallel, respectively, to the illumination direction. The resulting MCD spectrum is depicted in yellow.

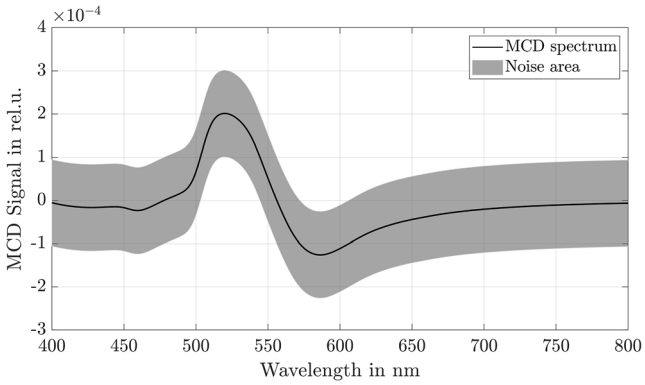

Figure 7. Calculated MCD spectrum for a 100 nm gold nanosphere and a magnetic field of 0.5 Tesla. The gray shaded area indicates the minimum precision required to detect an expected MCD spectrum. This precision corresponds to an SNR of 10^4 for the scattering spectrum of the gold nanosphere.

5.2. Experimental Results

To measure MCD in the dark-field spectrum of a gold nanosphere, a stack of N52 permanent disk magnets attached to a servo motor was assembled on top of the sample, as illustrated in Figure 3a. The magnetic field strength at the position of the gold nanospheres a few millimeters away roughly reaches 0.5 Tesla.

Bright-field and white-light dark-field illumination was used to detect the local plasmonic resonance of the single gold nanospheres using a cooled CCD camera or a color camera (see Figure 3). The polarization of the white-light illumination was controlled by a linear polarizer and a spectrometer measured the collected scattering spectrum. Right before the spectrometer a slit and a pinhole were placed to ensure that only the scattering from a single gold nanosphere is collected. A circular polarizer blocked one of the shifted spectra for each measurement. To reach the required SNR of 10^4 discussed above, the acquisition time was increased to 2000 s, the CCD camera was water-cooled, and a series of spectra were measured and averaged over. The sample was kept still for a few hours, then realignment and refocusing were performed. This technique showed a noticeable decrease in the drift. **Figure 8** presents the spectra of four consecutive acquisitions with the magnetic field reversed by 180° after each acquisition. Each spectrum is normalized to the spectrum of an Xe-lamp. The spectra with the same magnetic field direction were averaged and the MCD spectrum was calculated by taking the difference of two such sets with antiparallel field directions. **Figure 9** compares the measured MCD spectrum (green data points) to the theoretical one (solid black line, see Section 5.1).

At first glance, the experimental MCD spectrum matches the expected spectrum within experimental errors. However, we performed test experiments to exclude spectral artifacts and remaining sample drift. This is discussed in the following subsection.

5.3. Discussion and Estimation of Sensitivity

We performed a test for systematic errors by measuring the difference of two subsequently acquired dark-field spectra for identical orientations of the magnetic field. These are also plotted in Figure 9

© 2023 The Authors. physica status solidi (a) applications and materials science published by Wiley-VCH GmbH

18626319, 0, Downloaded from https://particles.particles-prod.literatumonline.com/doi/10.1002/pssa.202300380 by Helmholtz-Zentrum Berlin Für, Wiley Online Library on [12/12/2023]. See the Terms and Conditions (https://onlinelibrary.wiley.com/terms-and-conditions) on Wiley Online Library for rules of use; OA articles are governed by the applicable Creative Commons License

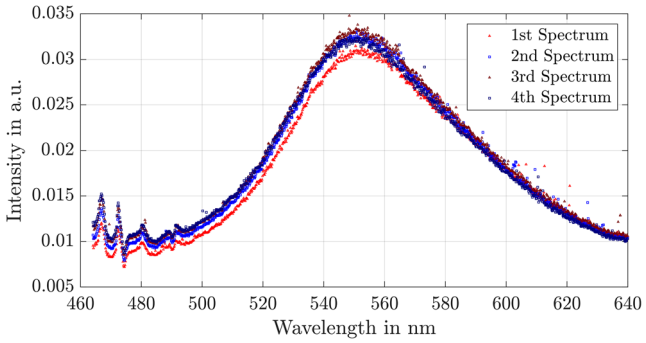

Figure 8. Dark-field scattering spectra of a single gold nanosphere in an external magnetic field with an exposure time of 2000 s. Spectra 1 and 3 are measured with the magnetic field parallel and spectra 2 and 4 antiparallel to the excitation laser beam, respectively.

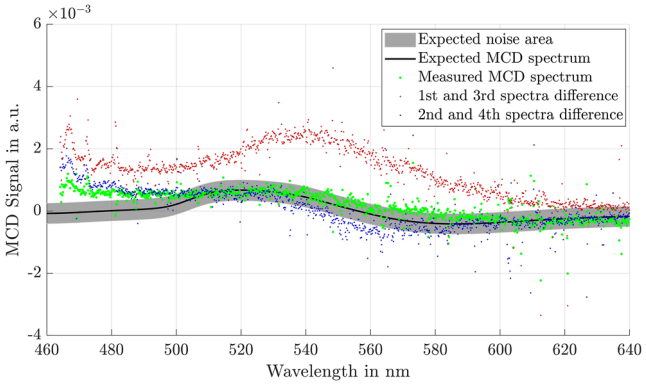

Figure 9. Measured MCD spectrum of a single gold nanosphere (green dots) compared to theoretical expectation (black solid line). The gray-shaded area indicates the precision required to detect an expected MCD. Differences in spectra with the same magnetic field direction are shown for 1st and 3rd (red dots) as well as 2nd and 4th spectra (blue dots).

as blue and red dots. These curves should be flat and centered around a horizontal line at zero. Obviously, there is a remaining drift within the acquisition time of the spectra leading to a deviation from the theoretically expected behavior. An analysis of the data revealed that the actual SNR for long acquisition times is on the order of 151, much less than the value of 10^4 required for the dark-field measurements. In conclusion, the SNR should be increased by an additional order of magnitude and the sample drift should be minimized to detect a magnetically induced MCD spectrum for a single bare gold nanosphere of 100 nm unambiguously. In the following section, we discuss an approach and provide first test measurements of how to overcome this issue with an enhancement of the magnetic response by using iron oxide nanoclusters.

6. Enhancement of Magnetic Response via Iron Oxide Nanoclusters

6.1. Conceptual Considerations

As rationalized in Section 3.2.2, hybrid particles consisting of a gold core surrounded by an iron oxide shell or vice versa may enhance the MCD of bare gold particles. Alternatively, a small nanocluster of iron oxide next to a gold nanosphere may serve the same purpose. We have shown in Section 4.1 that self-assembly of nanowires and nanoparticles in different material combinations is possible using a two-step self-assembly. Adding another self-assembly step could lead to the desired two-particle scheme, where a gold nanosphere next to an iron oxide nanocluster is attached to a nanowire. Unfortunately, the yield to find such a configuration is low. As described in this section, we thus concentrated on the influence of sole iron oxide nanoclusters on SPP transport in a nanowire in different configurations under the influence of a magnetic field. Such an effect was observed recently in a metal–insulator–metal waveguide side-coupled to a magneto-optical disk by Pae et al.[20] The configuration to achieve magnetically controlled routing as sketched on Figure 1 can also be used for a magnetic control of SPP transmission. A particle with MCD next to a plasmonic waveguide predominantly scatters SPPs with a certain circularly polarized field component in the near field. Therefore, if the MCD is controlled by an external magnetic field the propagation loss can be controlled as well.

6.2. Transport Studies on Iron Oxide Nanocluster-Waveguide Structures

An iron oxide nanocluster-nanowire configuration was assembled, as described in Section 4.1. A single system, as depicted in **Figure 10**a, was selected for further investigation. In the following experiments, we studied the transport of SPPs from a local excitation spot to a local collection spot. These are indicated by green and red circles, respectively, in the following figures. In the first configuration (Figure 10a), we looked for potential magnetic field dependence of directional coupling. A linearly polarized laser (532 nm) excited an iron oxide nanocluster attached to a silver nanowire. Mapping the propagation of SPPs was achieved via the detection of the Stokes-shifted fluorescence from encapsulated molecules in the silica shell of the silver nanowires after a long-pass filter. Upon illumination of the iron oxide nanoclusters (Figure 10b), the dye molecules in the nanowire encapsulation start bleaching, but reach a steady state after roughly 10 min. The SPPs decay exponentially while propagating, and dye molecules at the end facets experience less bleaching than the ones closer to the excitation spot. The fluorescence at the end facets therefore is proportional to the SPPs that propagated successfully to the wire ends. We detected this fluorescence in a series of 20 acquisitions with an exposure time of 60 s each. The magnet's position was rotated by 180° after each acquisition to observe potential different intensities at each nanowire end-facet. Another acquisition with the same exposure time to determine the background contribution was conducted and subtracted from each florescence image in the series. The Gaussian distributions of the fluorescence intensity at the excitation spot and at the two end facets (at left and right side of the nanowire) cover more than one pixel in the image, thus a 7×7 superpixel was chosen for each spot at the nanowire end facets. The intensities of all the pixels are integrated over to form a superpixel. Then, the integrated intensities were used to calculate the contrast of the end facet intensities

© 2023 The Authors. physica status solidi (a) applications and materials science published by Wiley-VCH GmbH

18626319, 0, Downloaded from https://pericles.pericles-prod.literatumonline.com/doi/10.1002/pssa.202300380 by Helmholtz-Zentrum Berlin Für, Wiley Online Library on [12/12/2023]. See the Terms and Conditions (https://onlinelibrary.wiley.com/terms-and-conditions) on Wiley Online Library for rules of use; OA articles are governed by the applicable Creative Commons License

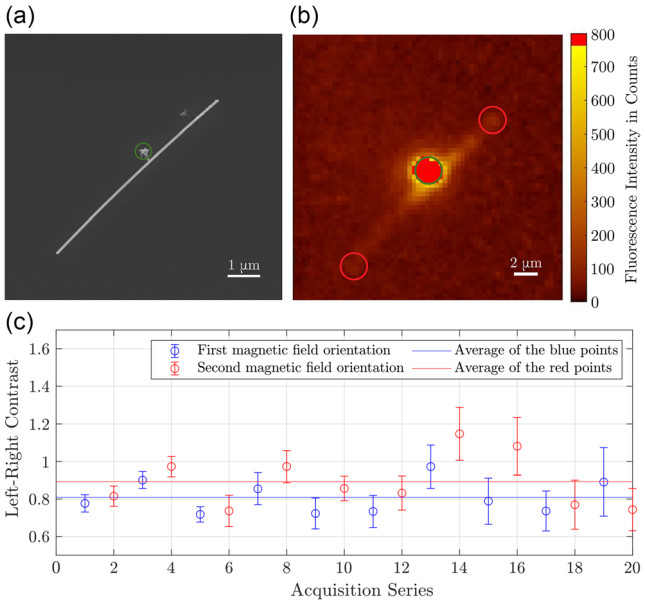

Figure 10. Investigation of potential magnetic field dependence on directional coupling. a) SEM image of a silver nanowire and an iron oxide nanocluster. b) Fluorescence microscopy image of the same system showing the excitation spot (green circle) and outcoupling spots at the end facets (red circles). c) Contrast of the intensities at left and right end facets, respectively, for two antiparallel orientations of the magnetic field. Horizontal lines indicate the average values.

$$\text{Contrast} = \frac{I_L - I_R}{I_L + I_R} \tag{1}$$

The errors ΔI_L and ΔI_R of the measured intensities I_L and I_R, respectively, are estimated via the standard deviation of the background image and calculated for the contrast through Gaussian error propagation formulas. The series of measurements is plotted in Figure 10c. Within the experimental errors, no dependence of the contrast on the direction of the magnetic field was found.

A second configuration of magnetic field-dependent SPP transport studies is shown in **Figure 11**. The laser excites SPPs at one of the end facets of the silver nanowire (green circles in Figure 11a) and the fluorescence scattered from the iron oxide nanocluster (red circle) is detected in the far field. In this device, the particle was found not in the middle of the nanowire, which allowed for studying two different propagation distances.

A series of 40 acquisitions each with an exposure time of 120 s was acquired. Each time the orientation of the magnetic field was rotated by 90°. The resulting fluorescence images were background subtracted and the noise for each spot was determined for every acquisition. Then, 3×3 superpixels are chosen and integrated over the Gaussian distribution of fluorescence around the outcoupling spot (indicated by a red circle). The smaller size of the superpixel decreases the noise level while containing the necessary information from the intensity distribution.

The experimental results are summarized in **Figure 12**. In a) the excitation laser was focussed on the end facet further away from the iron oxide nanocluster and fluorescence light scattered from the cluster (blue circles) and the mentioned end facet (red circles) was collected. Then the magnet was rotated by 90° and a next measurement was performed. The series of 40 measurements does not show a correlation with the orientation of the magnetic field. This is confirmed by a Fourier transform of the series, as shown in Figure 12b, where also no pronounced peak is observed. A similar series and Fourier analysis were performed when focussing the laser on the end facet closer to the iron oxide nanocluster (Figure 12c,d). Finally, a control measurement with no magnetic field applied (not shown) was done as well. In all series, no modification of plasmon transport through the nanowire decorated with the iron oxide nanocluster was detectable in our setup.

6.3. Discussion and Sensitivity Estimation

The experimental results in the previous section showed that an iron oxide nanocluster alone can act as a scatterer to couple SPPs in or out of a nanowire waveguide, but it does not modify SPP propagation under the presence of a magnetic field up to 0.5 Tesla. As pointed out in Section 5.1, a combination of iron oxide nanoclusters and noble metal nanospheres may boost the magnetic response. Based on the experimental parameters derived from the MCD and transport measurements, we performed a simulation to set a lower limit for the required enhancement of magnetically controlled transport of SPPs in our system. The geometry of the system is the same as the one depicted in Figure 11a with an iron oxide nanocluster coupled to a nanowire.

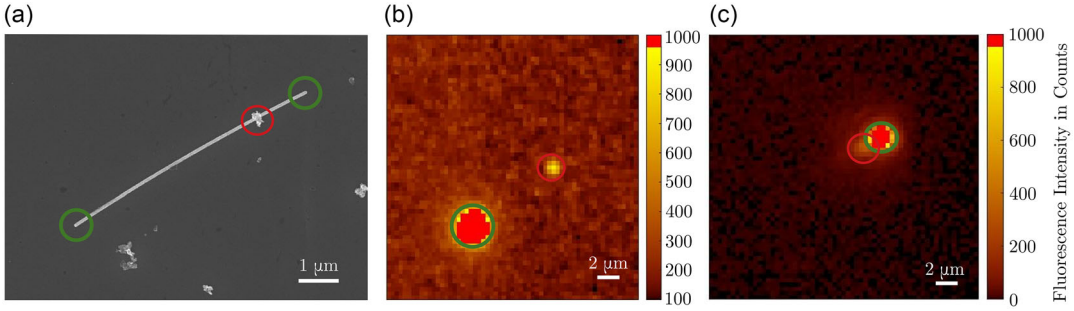

Figure 11. Investigation of potential magnetic field dependence of transport through nanowire. a) SEM image of the investigated silver nanowire and an iron oxide nanocluster attached. Excitation and collection spots are indicated by green and red circles, respectively. b,c) Fluorescence images of the same system, with laser excitation at the left and right end facets, respectively.

© 2023 The Authors. physica status solidi (a) applications and materials science published by Wiley-VCH GmbH

18626319, 0, Downloaded from https://particles.perichles-prod.literatumonline.com/doi/10.1002/pssa.202300380 by Helmholtz-Zentrum Berlin Für, Wiley Online Library on [12/12/2023]. See the Terms and Conditions (https://onlinelibrary.wiley.com/terms-and-conditions) on Wiley Online Library for rules of use; OA articles are governed by the applicable Creative Commons License

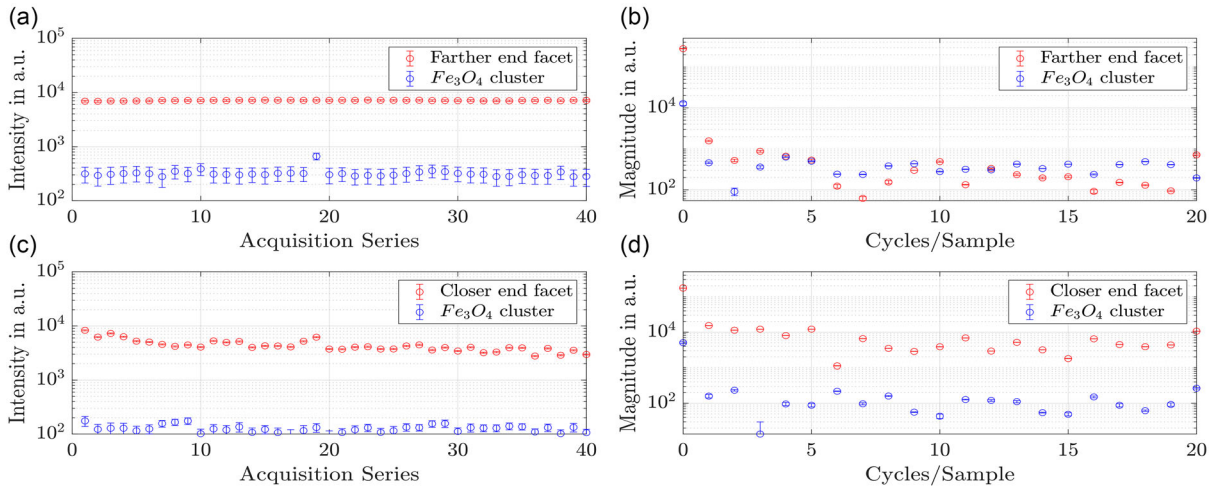

Figure 12. Analysis of magnetic field dependence of transport through a silver nanowire with different excitation conditions. a) Excitation on the end facet further away from the iron oxide nanocluster (see Figure 11) and collection of scattered fluorescence from the cluster (blue circles) and the same end facet (red circles). The absolute fluorescence intensities (arbitrary units) are shown. A series of 40 measurements was taken with the magnet rotated by 90° each time. b) Fourier transform of the series in (a). c,d) Same as (a,b) but with the excitation on the end facet closer to the iron oxide nanocluster.

SPP detection is performed by collection of the fluorescence emitted by molecules in the nanowire shell near its end facets and directly at the location of the nanocluster. Exponential damping of SPPs traveling along the wire from an excitation spot (at the end facets) to the collected fluorescence at the nanocluster (effective refractive index $n_{\text{eff}} = 1.77 - 0.01\,i$) is taken into account. The initial fluorescence intensity and the background Gaussian noise based on the experimentally derived parameters are added as well. A magnetically controlled transport is simulated heuristically by introducing an intensity difference ΔI_{mag} between the fluorescence intensity with and without the applied magnetic field at the collection spot. It is then assumed that the magnetic field is modulated periodically. The fluorescence intensity at one end facet (excitation spot) and at the Fe_3O_4 nanocluster (5.36 µm away from the excitation spot) is Fourier transformed. **Figure 13** shows the numerically generated data. The SNR of the Fourier component corresponding to the modulation frequency of the magnetic field is plotted as a function of the intensity difference ΔI_{mag} relative to the excitation intensity I_{Exc}. The simulation provides an estimation of the sensitivity of our setup to detect a magnetically induced modification of the SPP density, which is proportional to the detected molecular fluorescence intensity. The red dots in Figure 13 show the calculated Fourier component SNR as a function of the relative intensity difference $\Delta I_{\text{mag}}/_{\text{Exc}}$ collected right at the excitation spot at the wire's end facet. This curve somewhat quantifies the efficiency of our setup to detect SPPs via collection of fluorescence light from the molecules in the wire's shell. A value of approximately 1.4% for $\Delta I_{\text{mag}}/I_{\text{Exc}}$ is necessary to be above an SNR of 2. The blue dots line in Figure 13 shows $\Delta I_{\text{mag}}/I_{\text{Exc}}$ recorded at the location of the nanocluster when the SPPs have traveled 5.36 µm away from the excitation spot at the end facet. Due to exponential damping which is included in the simulation, the signal is much weaker, and thus the background noise is more pronounced. In this situation, a ten-time larger value of approximately 14% for $\Delta I_{\text{mag}}/I_{\text{Exc}}$ is necessary to achieve the same SNR of 2.

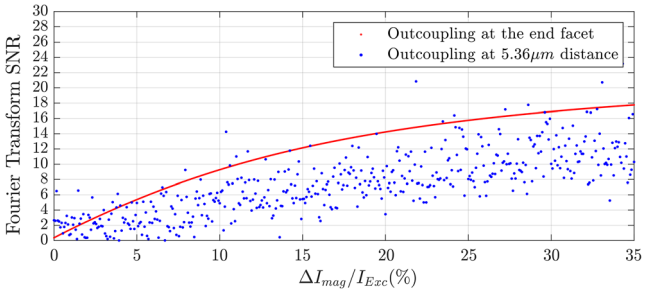

Figure 13. Simulated data showing the Fourier component as a function of the relative fluorescence intensity difference (see text) recorded at the location of excitation at the wire's end facet (red dots) and at the nanocluster 5.36 µm away from the excitation spot (blue dots). Due to the much weaker signal at the location of the nanocluster, the relative noise is enhanced. The configuration is as in Figure 11a.

Based on the simulated data, one can look back at the measured data in Figure 12b,d. The SNR provided by the experimental setting is smaller than 2. Therefore, no modulation of SPP propagation by the electric field, which would appear as a peak at a modulation frequency (20 cycles/sample) can be expected. We conclude that at least one order of magnitude improvement of the sensitivity of the setup or of the modulation strength to the magnetic field would be required.

7. Conclusion

We have demonstrated reliable and versatile self-assembly of hybrid devices consisting of nanoparticles (Au, Ag, iron oxide) coupled to a plasmonic nanowire. The phenomenon of spin-momentum locking (SML) can be observed with all these different nanoparticles. A setup was developed to study magnetic field-dependent SPP transport in combination with SML using a permanent magnet. We were able to isolate individual devices

© 2023 The Authors. physica status solidi (a) applications and materials science published by Wiley-VCH GmbH

18626319, 0, Downloaded from https://pericles.pericles-prod.literatumonline.com/doi/10.1002/pssa.202300380 by Helmholtz-Zentrum Berlin Für, Wiley Online Library on [12/12/2023]. See the Terms and Conditions (https://onlinelibrary.wiley.com/terms-and-conditions) on Wiley Online Library for rules of use; OA articles are governed by the applicable Creative Commons License

and perform SPP transport measurements in different configurations. In a setting with an iron oxide particle coupled to a silver nanowire, we looked for circular dichroism induced by a magnetic field and its potential effect on directional SPP generation or magnetic field-dependent transport. However, the effect was below the sensitivity threshold of our setup. To estimate the required sensitivity, we performed numerical simulations using a heuristic model based on the experimentally derived parameters. We found that at least an enhancement of one order of magnitude is required either of the sensitivity of our setup or of the modulation by the magnetic field. An immediate step to achieve this would be to use a much larger magnetic field. Since our experiments were limited to a magnetic field strength of 0.5 Tesla, a setup equipped with a few Tesla magnets would suffice. As another approach, we suggest the combination of plasmonic particles and, e.g., magnetic nanoparticles to locally enhance the magnetic field[55] and thus boost the magnetic response, e.g., MCD. Our approach of hybrid assembly would be ideal to investigate such systems with the goal to establish magnetically controlled functionality in nanoscale devices.

Supporting Information

Supporting Information is available from the Wiley Online Library or from the author.

Acknowledgements

Funding by the Deutsche Forschungsgemeinschaft (DFG), Project No. 182087777-SFB 951 (project B2) is acknowledged.

Open Access funding enabled and organized by Projekt DEAL.

Conflict of Interest

The authors declare no conflict of interest.

Data Availability Statement

The data that support the findings of this study are available from the corresponding author upon reasonable request.

Keywords

nanoparticles, plasmons, self-assembly, spin-momentum locking, waveguides

Received: May 18, 2023
Revised: July 30, 2023
Published online:

[1] C. Sayrin, C. Junge, R. Mitsch, B. Albrecht, D. O'Shea, P. Schneeweiss, J. Volz, A. Rauschenbeutel, *Phys. Rev. X* **2015**, *5*, 041036.
[2] M. Scheucher, A. Hilico, E. Will, J. Volz, A. Rauschenbeutel, *Science* **2016**, *354*, 1577.
[3] I. Söllner, S. Mahmoodian, S. L. Hansen, L. Midolo, A. Javadi, G. Kiršanskė, T. Pregnolato, H. El-Ella, E. H. Lee, J. D. Song, S. Stobbe, P. Lodahl, *Nat. Nanotechnol.* **2015**, *10*, 775.
[4] D. K. Gramotnev, S. I. Bozhevolnyi, *Nat. Photonics* **2010**, *4*, 83.
[5] W. B. Gao, A. Imamoglu, H. Bernien, R. Hanson, *Nat. Photonics* **2015**, *9*, 363.
[6] P. Lodahl, S. Mahmoodian, S. Stobbe, A. Rauschenbeutel, P. Schneeweiss, J. Volz, H. Pichler, P. Zoller, *Nature* **2017**, *541*, 473.
[7] S. Barik, A. Karasahin, C. Flower, T. Cai, H. Miyake, W. DeGottardi, M. Hafezi, E. Waks, *Science* **2018**, *359*, 666.
[8] L. Lu, J. D. Joannopoulos, M. Soljačić, *Nat. Photonics* **2014**, *8*, 821.
[9] A. B. Khanikaev, S. H. Mousavi, W. K. Tse, M. Kargarian, A. H. MacDonald, G. Shvets, *Nat. Mater.* **2013**, *12*, 233.
[10] K. W. Smith, L. A. McCarthy, A. Alabastri, L. Bursi, W. S. Chang, P. Nordlander, S. Link, *ACS Nano* **2018**, *12*, 11657.
[11] R. Schreiber, N. Luong, Z. Fan, A. Kuzyk, P. C. Nickels, T. Zhang, D. M. Smith, B. Yurke, W. Kuang, A. O. Govorov, T. Liedl, *Nat. Commun.* **2013**, *4*, 2948.
[12] N. J. Greenfield, *Nat. Protocols* **2007**, *1*, 2876.
[13] W. Paiva-Marques, F. Reyes Gómez, O. Oliveira, J. Mejía-Salazar, *Sensors* **2020**, *20*, 944.
[14] F. Neubrech, M. Hentschel, N. Liu, *Adv. Mater.* **2020**, *32*, 1905640.
[15] S.-H. Gong, F. Alpeggiani, B. Sciacca, E. C. Garnett, L. Kuipers, *Science* **2018**, *359*, 443.
[16] Q. Guo, T. Fu, J. Tang, D. Pan, S. Zhang, H. Xu, *Phys. Rev. Lett.* **2019**, *123*, 183903.
[17] M. Rothe, Y. Zhao, J. Müller, G. Kewes, C. T. Koch, Y. Lu, O. Benson, *ACS Nano* **2021**, *15*, 351.
[18] G. Armelles, A. Cebollada, A. García-Martín, M. U. González, *Adv. Opt. Mater.* **2013**, *1*, 10.
[19] B. Sepulveda, L. Lechuga, G. Armelles, *J. Lightwave Technol.* **2006**, *24*, 945.
[20] J. S. Pae, S. J. Im, K. S. Ho, C. S. Ri, S. B. Ro, J. Herrmann, *Phys. Rev. B* **2018**, *98*, 41406.
[21] K.-S. Ho, S.-J. Im, J.-S. Pae, C.-S. Ri, Y.-H. Han, J. Herrmann, *Sci. Rep.* **2018**, *8*, 10584.
[22] J. B. Khurgin, *Appl. Phys. Lett.* **2006**, *89*, 251115.
[23] V. Kuzmiak, S. Eyderman, M. Vanwolleghem, *Phys. Rev. B* **2012**, *86*, 045403.
[24] V. I. Belotelov, I. A. Akimov, M. Pohl, V. A. Kotov, S. Kasture, A. S. Vengurlekar, A. V. Gopal, D. R. Yakovlev, A. K. Zvezdin, M. Bayer, *Nat. Nanotechnol.* **2011**, *6*, 370.
[25] E. Ferreiro-Vila, J. M. García-Martín, A. Cebollada, G. Armelles, M. U. González, *Opt. Express* **2013**, *21*, 4917.
[26] J. B. González-Díaz, J. M. García-Martín, A. García-Martín, D. Navas, A. Asenjo, M. Vázquez, M. Hernández-Vélez, G. Armelles, *Appl. Phys. Lett.* **2009**, *94*, 263101.
[27] J. Petersen, J. Volz, A. Rauschenbeutel, *Science* **2014**, *346*, 67.
[28] A. Gabbani, G. Petrucci, F. Pineider, *J. Appl. Phys.* **2021**, *129*, 211101.
[29] B. Han, X. Gao, J. Lv, Z. Tang, *Adv. Mater.* **2020**, *32*, 1801491.
[30] F. Pineider, G. Campo, V. Bonanni, C. D. J. Fernández, G. Mattei, A. Caneschi, D. Gatteschi, C. Sangregorio, *Nano Lett.* **2013**, *13*, 4785.
[31] M. Artemyev, R. Krutokhvostov, D. Melnikau, V. Oleinikov, A. Sukhanova, I. Nabiev, in *Plasmonics: Metallic Nanostructures and their Optical Properties X*, Vol. *8457*, SPIE NanoScience + Engineering, San Diego, CA, United States **2012**, pp. 164–173, https://doi.org/10.1117/12.929860.
[32] Y. Izdebskaya, V. Shvedov, G. Assanto, W. Królikowski, *Nat. Commun.* **2017**, *8*, 14452.
[33] J. Estelrich, E. Escribano, J. Queralt, M. Busquets, *Int. J. Mol. Sci.* **2015**, *16*, 8070.
[34] P. K. Jain, Y. Xiao, R. Walsworth, A. E. Cohen, *Nano Lett.* **2009**, *9*, 1644.
[35] O. Benson, *Nature* **2011**, *480*, 193.
[36] A. W. Schell, G. Kewes, T. Schröder, J. Wolters, T. Aichele, O. Benson, *Rev. Sci. Instrum.* **2011**, *82*, 073709.

© 2023 The Authors. physica status solidi (a) applications and materials science published by Wiley-VCH GmbH

18626319, 0, Downloaded from https://pericles.pericles-prod.literatumonline.com/doi/10.1002/pssa.202300380 by Helmholtz-Zentrum Berlin Für, Wiley Online Library on [12/12/2023]. See the Terms and Conditions (https://onlinelibrary.wiley.com/terms-and-conditions) on Wiley Online Library for rules of use; OA articles are governed by the applicable Creative Commons License

[37] D. Englund, B. Shields, K. Rivoire, F. Hatami, J. Vučković, H. Park, M. D. Lukin, *Nano Lett.* **2010**, *10*, 3922, pMID: 20825160.
[38] D. V. Talapin, M. Engel, P. V. Braun, *MRS Bull.* **2020**, *45*, 799.
[39] Z. Li, Q. Fan, Y. Yin, *Chem. Rev.* **2022**, *122*, 4976, pMID: 34747588.
[40] M. Hu, J. Gao, Y. Dong, S. Yang, R. K. Li, *RSC Adv.* **2012**, *2*, 2055.
[41] Y. Sun, Y. Xia, *Science* **2002**, *298*, 2176.
[42] S. H. Im, Y. T. Lee, B. Wiley, Y. Xia, *Angew. Chem.* **2005**, *117*, 2192.
[43] X. Qi, K. A. Fichthorn, *Nanoscale* **2017**, *9*, 15635.
[44] Z. Chen, T. Balankura, K. A. Fichthorn, R. M. Rioux, *ACS Nano* **2019**, *13*, 1849.
[45] Z. Chen, J. W. Chang, C. Balasanthiran, S. T. Milner, R. M. Rioux, *J. Am. Chem. Soc.* **2019**, *141*, 4328.
[46] S. Jharimune, R. Pfukwa, Z. Chen, J. Anderson, B. Klumperman, R. M. Rioux, *J. Am. Chem. Soc.* **2021**, *143*, 184.
[47] M. Rothe, Y. Zhao, G. Kewes, Z. Kochovski, W. Sigle, P. A. van Aken, C. Koch, M. Ballauff, Y. Lu, O. Benson, *Sci. Rep.* **2019**, *9*, article no. 3859.
[48] M. Rothe, Y. Zhao, H. Halim, Y. Lu, O. Benson, *Opt. Continuum* **2022**, *1*, 1730.
[49] N. G. Bastús, J. Comenge, V. Puntes, *Langmuir* **2011**, *27*, 11098, pMID: 21728302.
[50] A. Gabbani, E. Fantechi, G. Petrucci, G. Campo, C. de Julián Fernández, P. Ghigna, L. Sorace, V. Bonanni, M. Gurioli, C. Sangregorio, F. Pineider, *ACS Appl. Nano Mater.* **2021**, *4*, 1057, pMID: 33778418.
[51] T. M. Chmereva, M. G. Kucherenko, *J. Appl. Spectrosc.* **2019**, *86*, 698.
[52] P. Tartaj, M. del Puerto Morales, S. Veintemillas-Verdaguer, T. González-Carreño, C. J. Serna, *J. Phys. D: Appl. Phys.* **2003**, *36*, R182.
[53] R. D. Deegan, O. Bakajin, T. F. Dupont, G. Huber, S. R. Nagel, T. A. Witten, *Nature* **1997**, *389*, 827.
[54] I. Mayergoyz, P. McAvoy, G. Lang, D. Bowen, C. Krafft, *J. Appl. Phys.* **2009**, *105*, 4.
[55] N. Sadzak, M. Héritier, O. Benson, *Sci. Rep.* **2018**, *8*, 8430.

© 2023 The Authors. physica status solidi (a) applications and materials science published by Wiley-VCH GmbH

18626319, 0, Downloaded from https://pericles.pericles-prod.literatumonline.com/doi/10.1002/pssa.202300380 by Helmholtz-Zentrum Berlin Für, Wiley Online Library on [12/12/2023]. See the Terms and Conditions (https://onlinelibrary.wiley.com/terms-and-conditions) on Wiley Online Library for rules of use; OA articles are governed by the applicable Creative Commons License